Aust. J. Phys., 1991, **44**, 15–32

Application of Melnikov's Method to the Reduced KdV Equation

J. Roessler

Department of Physics, University of Tasmania,
G.P.O. Box 252C, Hobart, Tas. 7001, Australia.

Abstract

The Melnikov method for estimating distances between invariant manifolds is applied to the perturbed system of ordinary differential equations obtained from the KdV equation, reduced by a travelling wave ansatz and including a diffusion term. The calculation is performed after one integration and the result is compared with numerical work carried out on the full system.

1. Introduction

Jeffrey and Kakutani (1972) have shown that soliton solutions of the Korteweg–deVries (KdV) equation are associated with homoclinic orbits in phase space. This association has been further developed by Holmes and Marsden (1981), as well as by Birnir (1988). Since the main application of the Melnikov method is to the splitting of the homoclinic orbit into stable and unstable manifolds due to perturbation of the nonlinear differential equation (Greenspan and Holmes 1983; Wiggins 1988), we have in this paper used the method to study the effect of periodic and dissipative perturbations on the KdV equation,

$$u_t + u_x u + u_{xxx} = 0\,. \tag{1}$$

To be more precise, we have extended equation (1) to the KdV–Burgers equation by allowing for a dissipation term proportional to u_{xx} and by adding an external force term that is periodic in space and time.

We shall in fact only be studying the 'reduced KdV equation' which arises when a travelling wave ansatz is made:

$$u(x,\, t) = u(x - ct) \equiv u(y)\,, \tag{2}$$

where c is the wave speed. In this way we are left with the reduced third-order ordinary differential equation (ODE),

$$u_{yyy} + u_y u - c u_y = 0\,. \tag{3}$$

0004-9506/91/010015$05.00

As explained by Olver (1986), the most general periodic solution to this equation after two integrations reads

$$u(y) = A\ \mathrm{cn}^2\,(\omega y + \delta) + M, \tag{4}$$

where the constants A, ω and M are actually interrelated and cn is the standard Jacobian elliptic function. It is called the 'cnoidal wave' solution. In the limit where the homoclinic orbit is approached and the elliptic modulus is $k \to 1$, the solution (4) degenerates to the form

$$u(y) = 3\ \mathrm{sech}^2\,(y/2 + \delta), \tag{5}$$

which is the 'soliton' or 'solitary wave' solution.

In Section 2 we apply a travelling wave ansatz to the KdV–Burgers equation under periodic forcing and analyse the phase portrait associated with the cnoidal and soliton solutions for the generalised KdV equation,

$$u_t + au_x u + bu_{xxx} = 0, \tag{6}$$

and discuss the effects of perturbations on the phase portrait.

In Section 3 the Melnikov integrals as well as the tangencies of manifolds and bifurcation curves are calculated. This section is guided by the well-known application of the Melnikov theory to the Duffing system by Greenspan and Holmes (1983) and by Guckenheimer and Holmes (1984). Section 4 presents the numerical work, such as plots of the manifolds in the phase portraits, and compares the computations with the calculations of Sections 2 and 3. The agreement is good.

2. Reduced KdV Equation

(a) Travelling Wave Reduction

We begin with a KdV–Burgers equation which is extended by an external periodic forcing term:

$$u_t + au_x u + bu_{xxx} + \delta u_{xx} + \alpha \cos\,(k_{\mathrm{p}} x - \omega t) = 0. \tag{7}$$

A travelling wave ansatz

$$y = x - ct, \qquad c = \omega/k_{\mathrm{p}} \tag{8}$$

reduces equation (7) to

$$-cu_y + au_y u + bu_{yyy} + \delta u_{yy} + \alpha \cos\,(k_{\mathrm{p}} y) = 0. \tag{9}$$

By redefining units of x and t, the wave speed c can be normalised to unity without loss of generality. Adopting this convention from now on and integrating equation (9) gives

$$-u + au^2/2 + bu_{yy} + \delta u_y + \alpha \sin\,(\omega y)/\omega = k_1, \tag{10}$$

where k_1 is an integration constant. This equation is our main object of analysis. To study it further we first find analytic solutions of (10) for vanishing dissipative and periodic forcing terms ($\alpha = \delta = 0$). These solutions are of course the travelling wave solutions of the KdV or MKdV equation and, after reintroducing small dissipative and periodic forcing terms ($1 > \alpha,\ \delta > 0$) as perturbations, we have the conditions necessary for Melnikov's method.

(b) Cnoidal and Soliton Solutions of the KdV Equation

The 'unperturbed' equation

$$-u + au^2/2 + bu_{yy} = k_1 \tag{11}$$

is obtained from (10) by setting $\alpha = \delta = 0$. Multiplying it by u_y, integrating and regrouping terms, leads to

$$\begin{aligned} u_y &= [-u^3 + 3u^2/a + 6k_1\, u/a + 6k_2/a]^{\frac{1}{2}}(a/3b)^{\frac{1}{2}} \\ &= [(u-r_1)(u-r_2)(r_3-u)]^{\frac{1}{2}}(a/3b)^{\frac{1}{2}}\,. \end{aligned} \tag{12}$$

The method of quadratures gives an elliptic integral (see e.g. Byrd and Friedman 1971,#236·00,p. 79) and consequently the cnoidal wave solution

$$u(y) = A\ \mathrm{cn}^2\, [\lambda(y-y_0),\, k] + r_2 \tag{13}$$

of the reduced KdV equation

$$-u_y + au_y\, u + bu_{yyy} = 0\,. \tag{14}$$

The abbreviations in (13) are as follows:

$$\begin{aligned} A &= r_3 - r_2, \qquad \lambda = [a(r_3-r_1)/3b]^{\frac{1}{2}}/2, \\ y_0 &= \text{arbitrary phase shift}, \\ k &= [(r_3-r_2)/(r_3-r_1)]^{\frac{1}{2}} = \text{elliptic modulus}. \end{aligned} \tag{15}$$

In the limit $k \to 1$ the solution (13) reduces to

$$u(y) \to A\ \mathrm{sech}^2\, [\lambda(y-y_0)] + r_2\,, \tag{16}$$

which is the solution of the KdV equation. We further note in this limit that

$$\begin{aligned} r_1 &= r_2\,, & r_3 &= 3/a - 2r_1\,, \\ k_1 &= ar_1^2/2 - r_1\,, & k_2 &= r_1^2/2 - ar_1^3/3\,. \end{aligned} \tag{17}$$

These relations are easily derived by matching powers of u in $(u-r_1)^2(r_3-u)$ with those in the polynomial of (12).

(c) Phase Space of the Reduced KdV Equation

In order to investigate the phase space of equation (14), within which the solutions (13) and (16) prevail, we represent (14) as a three-dimensional system of first order equations:

$$u_y = u_1\,,\quad u_{1y} = u_2\,,\quad u_{2y} = (1 - au)u_1/b\,. \tag{18}$$

Clearly, the complete set of fixed points (u_s, u_{1s}, u_{2s}) of this system is the entire u axis in the phase space spanned by u, u_1, u_2. Moreover, it is trivial to verify that the system (18) linearised about any of these fixed points has at least one eigenvalue equal to zero (all three eigenvalues are zero for $au_s = 1$); the fixed points become degenerate. This means that the problem of degenerate fixed points for the (unreduced) KdV equation as noted by Birnir (1988) carries over to the reduced version (14) or (18) respectively.

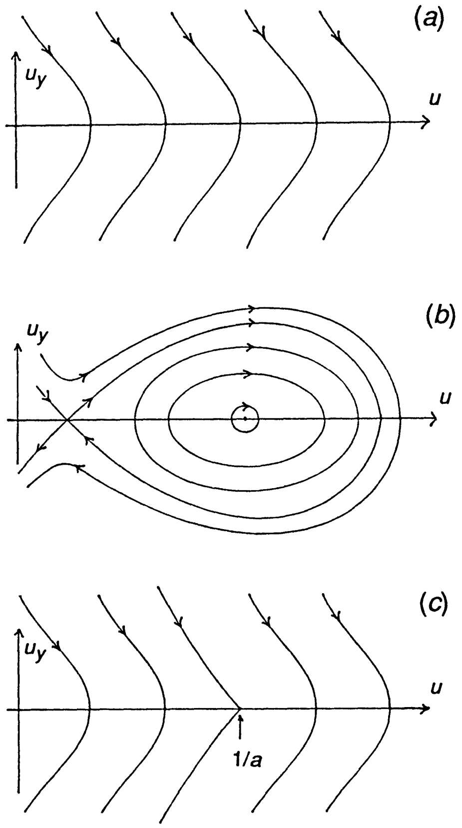

Fig. 1. Vector fields in the phase space of system (19): (*a*) case $k_1 < -1/2a$; (*b*) case $k_1 > -1/2a$; (*c*) case $k_1 = -1/2a$.

The situation changes, however, with the two-dimensional system arising from (11) integrated once more,

$$u_y = u_1 \qquad u_{1y} = (k_1 + u - au^2/2)/b\,. \tag{19}$$

Its fixed points (u_s, u_{1s}) in u–u_1 space are

$$u_{1s} = 0, \qquad u_{s\pm} = [1 \pm (1 + 2ak_1)^{\frac{1}{2}}]/a\,, \tag{20}$$

with eigenvalues

$$\lambda_{\pm} = \pm[(1 - au_{s\pm})/b]^{\frac{1}{2}} = \pm[\pm(1 + 2ak_1)^{\frac{1}{2}}/b]^{\frac{1}{2}}. \tag{21}$$

Depending on the integration constant k_1, three topologically distinct cases are possible for the phase portrait:

$$\text{Case 1}: \qquad k_1 < -1/2a. \tag{22}$$

Equation (21) shows that there are no real zeros for $u_{s\pm}$ and thus no fixed points for the system (19); see Fig. 1*a*.

$$\text{Case 2}: \qquad k_1 > -1/2a. \tag{23}$$

Equations (20) and (21) produce a saddle at $(u_{s-}, 0)$ and a centre at $(u_{s+}, 0)$; see Fig. 1*b*. According to (20) the distance d between them is

$$d = 2(1 + 2ak_1)^{\frac{1}{2}}/a. \tag{24}$$

$$\text{Case 3}: \qquad k_1 = -1/2a. \tag{25}$$

The distance d between saddle and centre is zero and so is the eigenvalue λ. This corresponds to a doubly degenerate Hamiltonian bifurcation in the terminology of Greenspan and Holmes (1983). The position of this degenerate fixed point is $1/a$; see Fig. 1*c*.

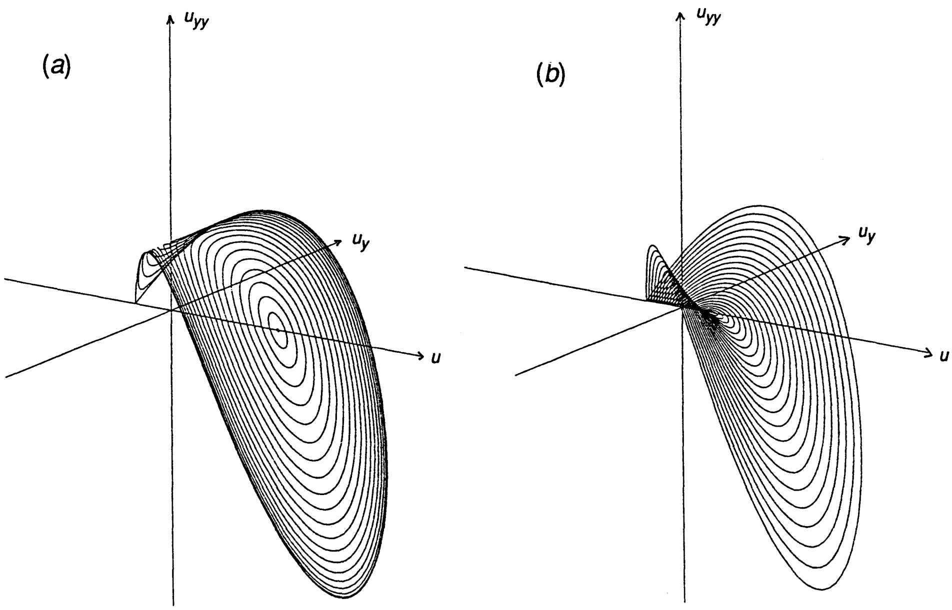

Fig. 2. (*a*) A family of periodic orbits on a parabolically curved invariant surface in the phase space of system (18) enclosed by a homoclinic orbit. (*b*) Set of homoclinic orbits in the phase space of system (18).

The phase diagram for the original three-dimensional system (18) can now be easily constructed. First, we add the dimension $u_2 = u_{yy}$ to the two-dimensional phase diagram of the system (19). Then, in any section parallel to the u–u_2 plane, there is a family of parabolas defined by (11) and continuously parametrised by k_1. Each one of these parabolas defines a surface P parallel to the u_1 $(= u_y)$ axis in u–u_1–u_2 space. Every such surface contains a phase portrait topologically equivalent to one of the three possible cases described by (22), (23) and (25). The specification of these three cases is:

Case 1. The surface P is bounded away from the u axis.

Case 2. The surface P is penetrated by the u axis at the saddle and centre of the phase portrait contained on P.

Case 3. The surface P touches the u axis exactly where saddle and centre of the phase portrait on P merge.

Figs 2*a* and 2*b* elucidate this geometry.

(d) Analytical Solutions and the Phase Portrait

We briefly comment on the three configurations above and on their connection to the analytic solutions mentioned in Section 2*b*. The vital quantity is the polynomial in (12) with roots r_1, r_2, r_3:

Case 1: The polynomial has one real and two complex conjugate roots.

Case 2: The three roots are real, which corresponds to the cnoidal and soliton solutions. It is clear that the cnoidal solutions (13) define the family of closed orbits, concentric to the centre $(u_{s+}, 0)$ and parametrised by the elliptic modulus k (see equation 15), whereas the homoclinic orbit connected to the saddle $(u_{s-}, 0)$ and enclosing the concentric orbits provides the soliton solution (16).

Case 3: The three real roots coalesce at $u = 1/a$. Centre and saddle meet there.

(e) Phase Space of the Reduced KdV Equation under Perturbations

Now we include the dissipation term and the periodic perturbation before investigating the phase space of equation (9), expressed as the three-dimensional first-order system:

$$\begin{aligned} u_y &= u_1, \qquad u_{1y} = u_2\,, \\ u_{2y} &= (1 - au)u_1/b - \delta u_2/b - \alpha\cos(\omega y)/b\,. \end{aligned} \tag{26}$$

In particular, we examine the effect of perturbations on the parabolically bent invariant surfaces P introduced in Section 2*c*. The set of P is now defined by equation (10) and, as opposed to the unperturbed case, each surface of P has a slope of value δ in the u_1 direction, induced by the dissipation term δu_y in (10). The periodic forcing term induces a y-periodic oscillation of the set of P with frequency ω and amplitude α/b along the u_{yy} axis. It is important to note that, despite these perturbations, a point in phase space representing system (9) remains on its particular surface P for all times. This indicates that the phenomenon of Arnold diffusion does not happen.

3. Perturbations and the Melnikov Method

(a) Melnikov Integral of the Reduced and Perturbed KdV Equation

We begin by expressing equation (10) as a two-dimensional first-order system of ODEs:

$$\begin{aligned} u_y &= u_1\,, \\ u_{1y} &= (-au^2/2 + u + k_1)/b - \delta u_1 - \alpha \sin(\omega y)/\omega\,, \end{aligned} \tag{27}$$

after rescaling $\delta \to \delta/b$, $\alpha \to \alpha/b$. From hereon we will only work with this rescaled equation.

We recall that for a system such as

$$\begin{aligned} u_t &= f_1(u, v) + \epsilon g_1(u, v, t)\,, \\ v_t &= f_2(u, v) + \epsilon g_2(u, v, t)\,; \\ u &= u(t - t_0), \qquad v = v(t - t_0)\,, \\ g_i(u, v, t) &= g_i(u, v, t + T), \quad i = 1, 2\,, \end{aligned} \tag{28}$$

with ϵ as the perturbation parameter, t_0 a phase factor and T the period of the perturbation (g_1, g_2), the Melnikov integral $M(t_0)$ applicable to the solutions representing the homoclinic orbits of (28) is defined as

$$M(t_0) = \int_{-\infty}^{\infty} (f_1\, g_2 - f_2\, g_1)\, \mathrm{d}t\,. \tag{29}$$

System (27) is the system (19) with perturbation added, and comparison with the system (28) therefore shows that

$$\begin{aligned} f_1 &= u_1, & \epsilon g_1 &= 0\,, \\ f_2 &= (-au^2/2 + u + k_1)/b, & \epsilon g_2 &= -\delta u_1 - \alpha \sin(\omega y)/\omega\,. \end{aligned} \tag{30}$$

Introducing one more rescaling $\epsilon g_2 \to g_2$, and observing that y plays the role of time t, the homoclinic Melnikov integral becomes

$$\begin{aligned} M(y_0) &= \int_{-\infty}^{\infty} u_1\, g_2\, \mathrm{d}y = \int_{-\infty}^{\infty} u_y[-\delta u_y - (\alpha/\omega) \sin(\omega y)]\, \mathrm{d}y \\ &= -\delta \int_{-\infty}^{\infty} u_y^2\, \mathrm{d}y + \alpha \int_{-\infty}^{\infty} u \cos(\omega y)\, \mathrm{d}y - \alpha \sin(\omega y)/\omega \Big|_{-\infty}^{\infty} \\ &= -\delta \int_{-\infty}^{\infty} \{-2\lambda A\, \mathrm{sech}^2\, [\lambda(y - y_0)] \tanh[\lambda(y - y_0)]\}^2\, \mathrm{d}y \\ &\quad + \alpha A \int_{-\infty}^{\infty} \mathrm{sech}^2\, [\lambda(y - y_0)] \cos(\omega y)\, \mathrm{d}y\,. \end{aligned} \tag{31}$$

Here we have integrated by parts and substituted the soliton solution (16). After shifting $y \to y + y_0$ and applying some basic trigonometric identities the two integrals can be found in Gradshteyn and Ryzhik (1965) (p. 96,#2.416.1; p. 505,#3.982.1):

$$M(y_0) = 16\delta\lambda A^2/15 - \alpha A\pi\omega \cos(\omega y_0)/\lambda^2 \sinh[\pi\omega/(2\lambda)]. \tag{32}$$

According to the definition for the subharmonic Melnikov integral $M^{m/n}(t_0)$ of (28)

$$M^{m/n}(t_0) = \int_0^{mT} (f_1 g_2 - f_2 g_1)\, dy, \tag{33}$$

with $nT_k = mT$, n, m being coprime integers and T_k the period of the unperturbed ($\epsilon = 0$) periodic solutions of (28), we obtain in similar fashion

$$\begin{aligned} M^{m/n}(y_0) = \int_0^{mT} f_1 g_2\, dy &= -aA\int_0^{mT} \mathrm{cn}^2(\lambda y)\cos[\omega(y+y_0)]\, dy \\ &\quad -4\delta\lambda^2 A^2 \int_0^{mT} \mathrm{sn}^2(\lambda y)\,\mathrm{cn}^2(\lambda y)\,\mathrm{dn}^2(\lambda y)\, dy \\ &= -\alpha A I_{\mathrm{p}} - 4\delta\lambda^2 A^2 I_{\mathrm{d}}. \end{aligned} \tag{34}$$

We have substituted the cnoidal wave solution (13) here. The integral I_{p}, denoting the periodic part of $M^{m/n}$, is evaluated using a Fourier expansion of $\mathrm{dn}^2 = 1 - k^2 - k^2\mathrm{cn}^2$, as given in Greenhill (1892) (p. 286,#49):

$$\begin{aligned} I_{\mathrm{p}} &= \int_0^{mT} [k^2 - 1 + \mathrm{dn}^2(\lambda y)/k^2] \\ &\qquad \times [\cos(\omega y)\cos(\omega y_0) - \sin(\omega y)\sin(\omega y_0)]\, dy \\ &= \int_0^{mT} \Big(k^2 - 1 + E(k)/K(k) + [\pi^2/K^2(k)]. \\ &\qquad \times \sum_j j\cos[j\pi\lambda y/K(k)]/\sinh[j\pi K(k')/K(k)] \Big) \\ &\qquad \times [\cos(\omega y)\cos(\omega y_0) - \sin(\omega y)\sin(\omega y_0)]/k_2\, dy. \end{aligned} \tag{35}$$

Here K, E are the first and second elliptic integrals and $k'^2 = 1 - k^2$. Due to orthogonality of circular functions the only nonzero term in the integral (35) is

$$\left(j\pi^2 \cos(\omega y_0)/K^2(k)k^2 \sinh[j\pi K(k')/K(k)] \right) \int_0^{mT} \cos[j\pi\lambda y/K(k)]\cos(\omega y)\, dy, \tag{36}$$

if and only if the orthogonality condition

$$j\pi\lambda/K(k) = \omega \tag{37}$$

applies. Otherwise all terms vanish. From (37) and the resonance condition

$$mT = nT_k \quad \text{with} \quad T = 2\pi/\omega, \quad T_k = 2K(k)/\lambda, \tag{38}$$

we find that

$$j\pi\lambda/K(k) = \omega = m\pi\lambda/nK(k) \quad \text{or} \quad j = m/n. \tag{39}$$

In other words, for the indices j to be integer, we have the condition

$$n = 1. \tag{40}$$

The integral I_{p} therefore collapses to

$$I_{\mathrm{p}} = \omega\pi \cos(\omega y_0)/\lambda^2 k^2 \sinh[\omega K(k')/\lambda]. \tag{41}$$

The dissipation part I_{d} can be similarly evaluated using Gradshteyn and Ryzhik (1965) (p. 630, #5.134.3). The Melnikov integral then becomes

$$\begin{aligned} M^m(y_0) = {} & A\alpha\omega\pi \cos(\omega y_0)/\lambda^2 k^2 \sinh[\omega K(k')/\lambda] \\ & + 16A^2\lambda\delta[(1-k^2)(k^2-2)K(k) + (k^4-k^2+1)E(k)]/15k^4. \end{aligned} \tag{42}$$

Note that k is a function of m, such that

$$k(m \to \infty) \to 1, \tag{43}$$

and the homoclinic limit is correctly reached for $k \to 1$:

$$M^m(y_0) \to M(y_0). \tag{44}$$

(b) Tangencies and Quadratic Zeros

From (32) it is clear that the homoclinic Melnikov function $M(y_0)$ has quadratic zeros for $\cos(\omega y_0) = 1$. Therefore, the invariant manifolds W^s and W^u must have tangency points, and we define the tangency ratio $R(\omega)$ for $\alpha = \alpha_{\mathrm{c}}$ and $\delta = \delta_{\mathrm{c}}$:

$$R(\omega) = \alpha_{\mathrm{c}}/\delta_{\mathrm{c}} = 16A\lambda^3 \sinh(\pi\omega/2\lambda)/15\pi\omega. \tag{45}$$

The significance of this ratio can now be expressed in the form:

$$\begin{aligned} \alpha/\delta > R(\omega) \quad & \Leftrightarrow \quad W^s \wedge W^u \neq 0 \text{ (transverse intersection)}, \\ \alpha/\delta = R(\omega) \quad & \Leftrightarrow \quad W^s \wedge W^u \neq 0 \text{ (tangency)}, \\ \alpha/\delta < R(\omega) \quad & \Leftrightarrow \quad W^s \wedge W^u = 0. \end{aligned} \tag{46}$$

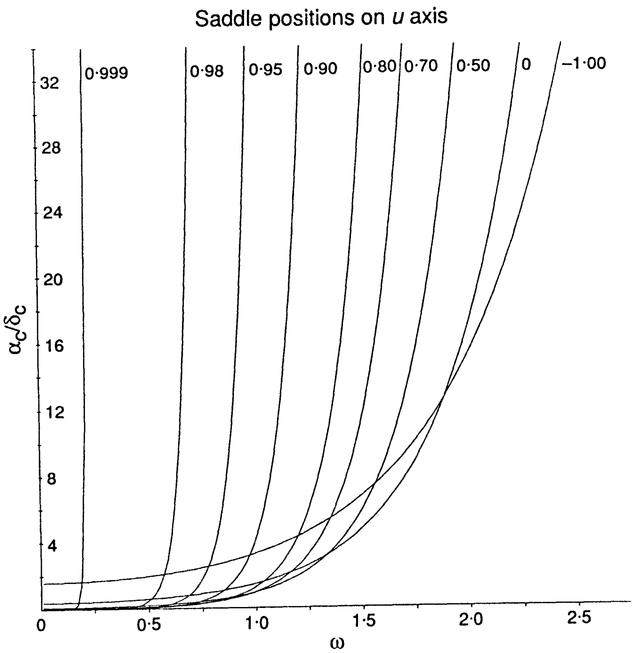

Fig. 3. Bifurcation curves in α_c/δ_c versus ω for various saddle positions.

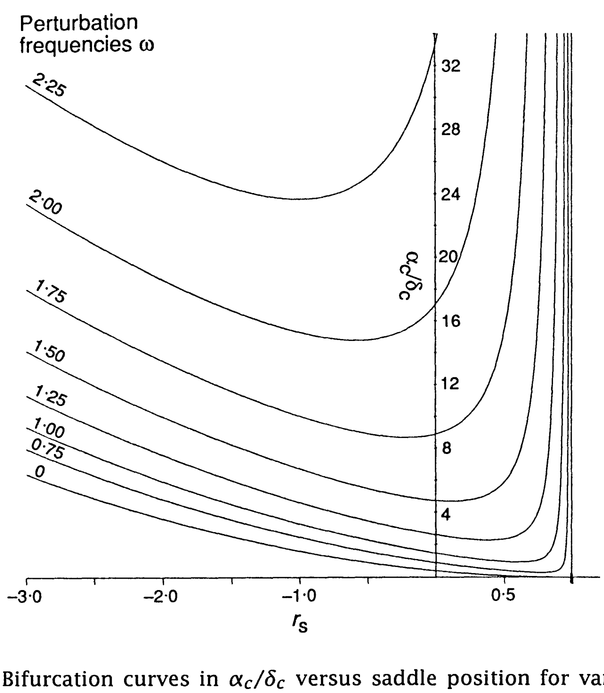

Fig. 4. Bifurcation curves in α_c/δ_c versus saddle position for various ω.

By using (17) and (15), A and λ can be replaced in (45) and $R(\omega)$ can be rewritten in terms of the coefficients a, b and the saddle position r_s $(= r_1 = r_2)$ on the u axis:

$$R(\omega) = 2bB^5 \sinh(\pi\omega/B)/5a\pi\omega; \qquad B = [(1 - ar_s)/b]^{\frac{1}{2}}. \tag{47}$$

The limit cases are

$$\begin{aligned} &R(\omega = 0) = 2bB^4/5a, \\ &r_s = 1/a \text{ (saddle and centre merge)}: \quad R(\omega \neq 0) = \infty \\ &\qquad\qquad\qquad\qquad\qquad\qquad\qquad\quad R(\omega = 0) = 0. \end{aligned} \tag{48}$$

Figs 3 and 4 show the bifurcation curves of R versus ω and versus the saddle position r_s respectively.

The critical ratio α_c/δ_c at which saddle-node bifurcations occur is determined from the subharmonic Melnikov function (42),

$$\begin{aligned} R^m(\omega) = 16A\lambda^3[2(1-k^2)(k^2-2)K(k) \\ + (k^4 - k^2 + 1)E(k)] \sinh[\omega K(k')/\lambda]/15\pi\omega k^2. \end{aligned} \tag{49}$$

This can also be rewritten in terms of a, b and m. We find through (15) and the resonance condition (38) that

$$A = 12\lambda^2 k^2 b/a, \qquad \lambda = \omega K(k)/\pi m, \tag{50}$$

$$\begin{aligned} R^m(\omega) = 64\omega^4 K^5(k) b[(1-k^2)(k^2-2)K(k) \\ + (k^4 - k^2 + 1)E(k)] \sinh[\pi m K(k')/K(k)]/5\pi^6 m^5 a. \end{aligned} \tag{51}$$

The function $R^m(\omega)$ can now be interpreted as the subharmonic version of (46):

$$\begin{aligned} \alpha/\delta > R^m(\omega) \quad &\Leftrightarrow \quad \text{resonance}, \\ \alpha/\delta = R^m(\omega) \quad &\Leftrightarrow \quad \text{saddle node bifurcation}, \\ \alpha/\delta < R^m(\omega) \quad &\Leftrightarrow \quad \text{quasiperiodicity}. \end{aligned} \tag{52}$$

Since the functional dependence of k on m is rather complicated due to the dependence of λ on k through the roots r_1, r_2, r_3—as can be seen from (50) and (15)—the critical ratio α_c/δ_c at which bifurcations occur cannot be determined by straightforward application of (51). The evaluation of R^m as given by (51) is described in the Appendix and examples of the resulting bifurcation curves for various resonance orders m are shown in Fig. 5.

4. Numerical Calculations and Computer Graphics

With the exception of Figs 1, 3, 4 and 5, the plots in all figures were produced by the application of the Runge–Kutta–Fehlberg FORTRAN ODE solver RKF45 (Shampine *et al.* 1976) on the three-dimensional system (18) or its perturbed version (26). Invariant manifolds are graphed in Figs 6 and 7 for

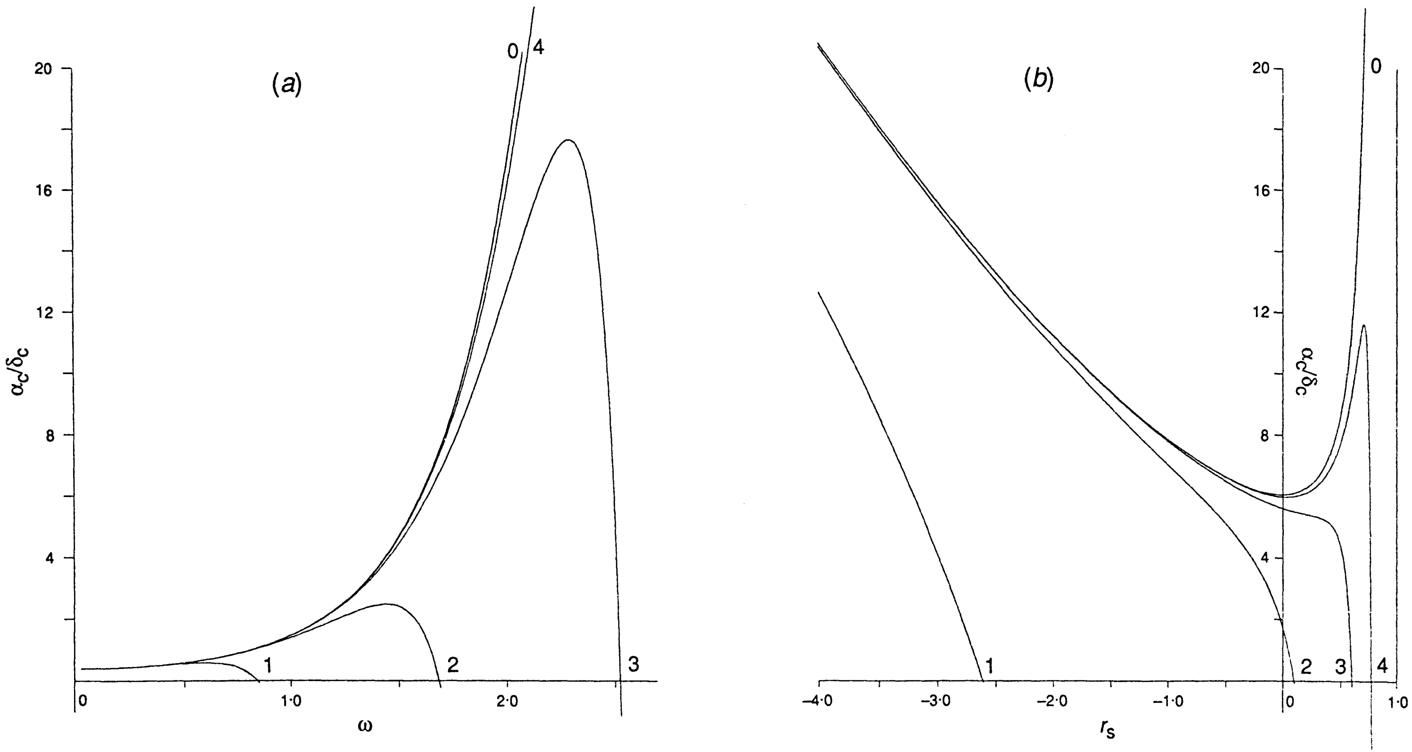

Fig. 5. Subharmonic bifurcation curves of the order indicated and their homoclinic limit (label 0) in α_c/δ_c versus ω. The saddle is at $u = 0$. The fourth order curve has a peak of $\alpha_c/\delta_c \approx 160$. (*b*) Same as (*a*), but for α_c/δ_c versus saddle position, with $\omega = 1 \cdot 60$.

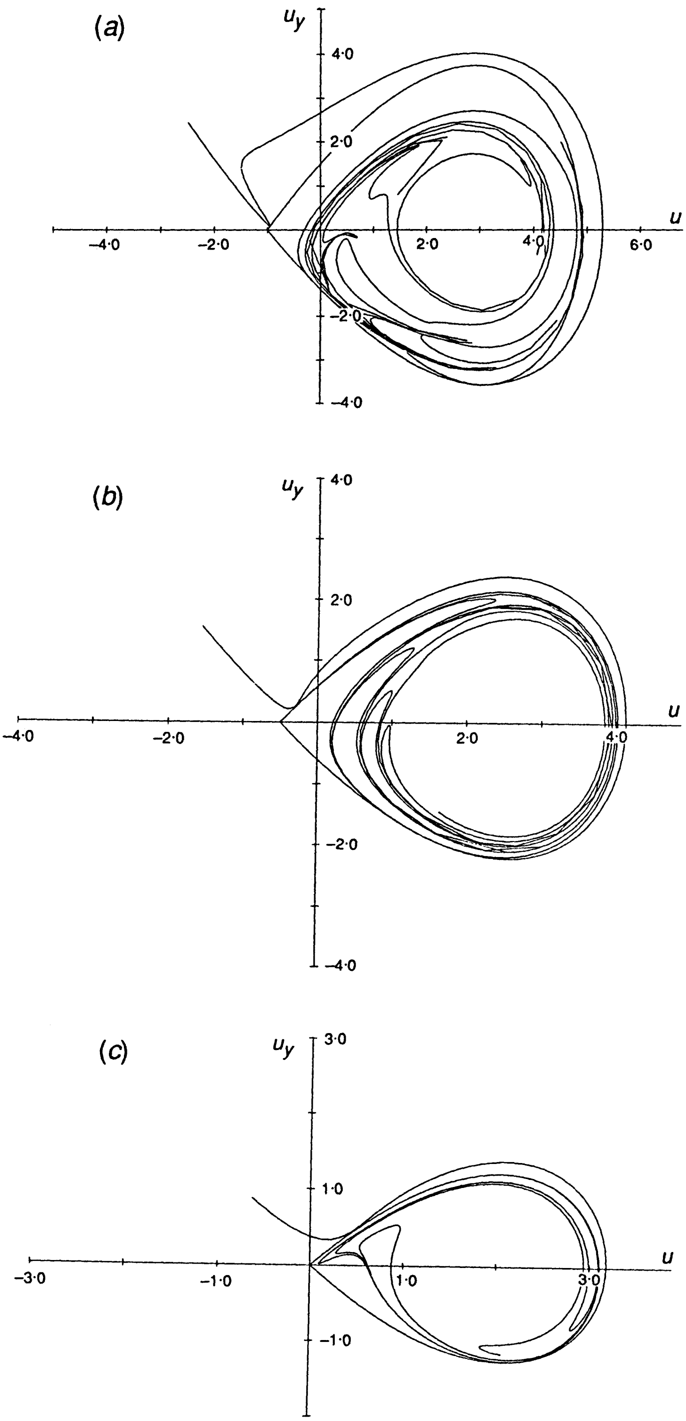

Fig. 6. Invariant manifolds for saddle at (*a*) $u = -1$, $\omega = 1$, $\alpha = 0 \cdot 17$, $\delta = -0 \cdot 05$, MR $= 3 \cdot 2815$; (*b*) $u = -0 \cdot 5$, $\omega = 1 \cdot 2$, $\alpha = 0 \cdot 064$, $\delta = -0 \cdot 02$, MR $= 3 \cdot 1682$; and (*c*) $u = 0$, $\omega = 1 \cdot 5$, $\alpha = 0 \cdot 095$, $\delta = -0 \cdot 02$, MR $= 4 \cdot 7241$.

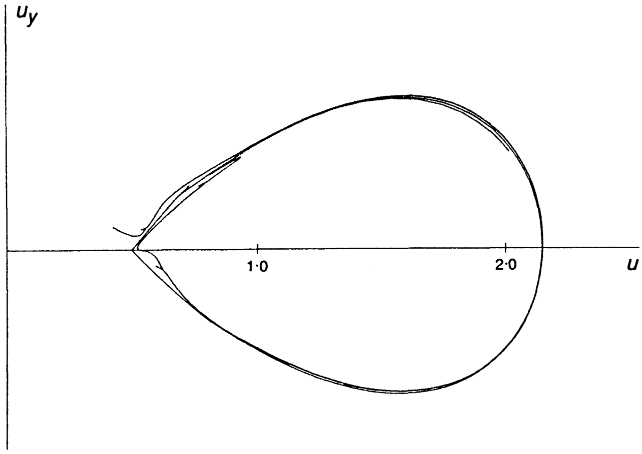

Fig. 7. Invariant manifolds for saddle at $u = 0 \cdot 5$, $\omega = 2$, $\alpha = 0 \cdot 081$, $\delta = -0 \cdot 002$ and $\mathrm{MR} = 40 \cdot 6738$.

$a = b = 1$ and for saddle positions on the u axis with perturbation frequencies ω, amplitudes α and dissipation coefficients δ as given in the captions. These values are about the lowest frequencies and largest perturbations which show tangencies and for which reasonable agreement with the critical ratio α_c/δ_c calculated from (47) (included in the captions as MR) could be achieved. An exception is set by the graph of Fig. 7 with saddle position $u = 0 \cdot 5$. Since this value is close to the saddle centre merging point $u = 1/a$, numerical errors become significant and the applicability of the Melnikov method as a first-order approximation becomes questionable, evidenced by the large perturbation values for α needed to produce tangency (see Figs 3 and 4).

In practical terms, the graphs for the invariant manifolds are generated by starting with a point p_i with coordinates $(u_i, 10^{-6}, 0)$. There u_i is the saddle position on the u axis with an offset by 10^{-6} from the u axis; the offset is needed to obtain a finite displacement of p_i under the Poincaré map $p_i \rightarrow P(p_i)$, which is then performed by advancing p_i by a timestep equal to the perturbation period $T = 2\pi/\omega$. A good approximation for the initial line element on the invariant manifold W^u (or W^s respectively by using negative time) can now be obtained by generating further points using p_i as the initial condition and solving the perturbed system (26) for $\alpha = 0$ and small timesteps. The stepsize is decreased exponentially with respect to the number of steps performed in order to compensate for the 'stretching' of the manifold under increasing time. After about 200 to 300 timesteps the set of points so generated will have reached a small enough neighbourhood of $P(p_i)$ to stop the process and readjust the resulting line of points to pass directly through $P(p_i)$. Further iterations of this line element assemble the invariant manifold and are generated by simply Poincaré mapping its individual points. It is evident from this method that the shorter this initial line element is, the better the approximation of the manifold will be. This explains why higher frequencies ω are needed to analyse smaller homoclinic orbits and enlightens the problem described in connection with Fig. 7.

The graphs showing the projections of the perturbed manifolds into the u_{yy}–u_y plane and the u_{yy}–u plane, as well as the perspective view (Figs 8 and 9), give numerical evidence of the properties described in Section 2*e*, such as invariant surfaces of parabolic curving and slopes in the direction of the u_y axis with values equal to the dissipation coefficient δ.

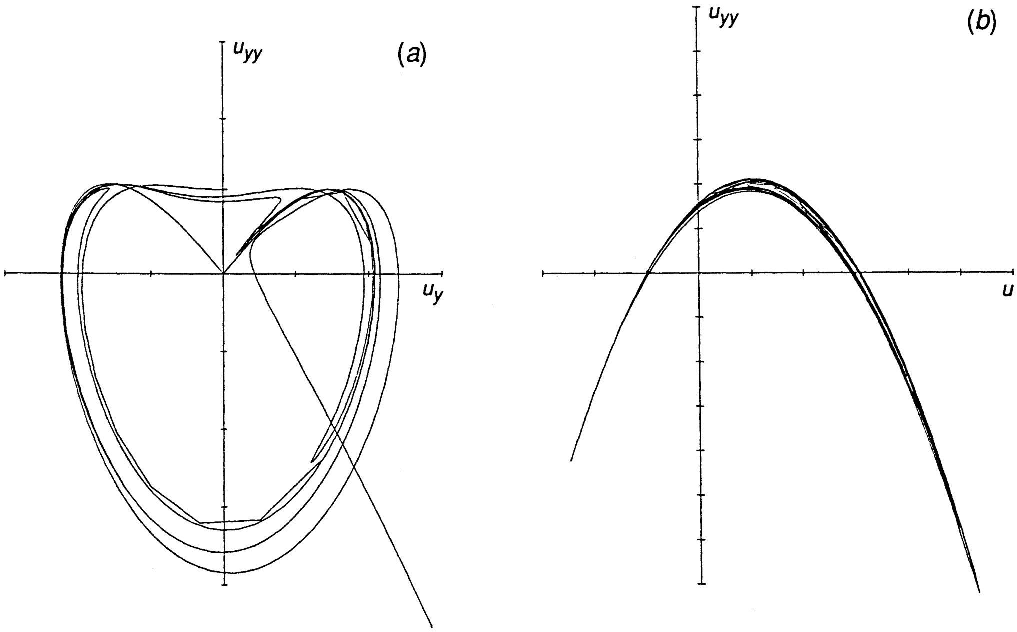

Fig. 8. Projection of the invariant manifolds into (*a*) the u_y–u_{yy} plane and (*b*) the u–u_{yy} plane.

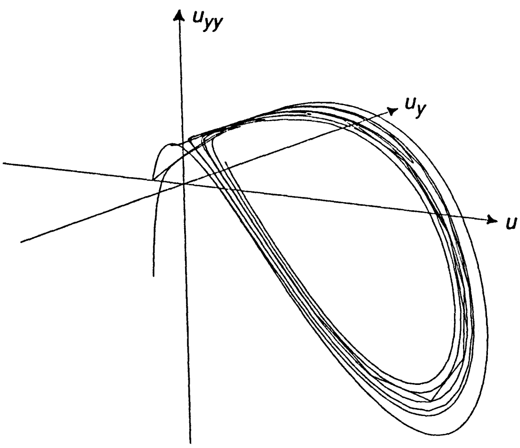

Fig. 9. Invariant manifolds in the u–u_y–u_{yy} phase space.

As there is only one homoclinic orbit connected to each saddle, solutions outside this homoclinic orbit must grow or decrease unbounded. As a consequence, only temporary or intermittent chaos is possible for the perturbed system. If the initial conditions are too far from the original centre of the unperturbed system, the solution will, after a few chaotic oscillations, decrease unbounded. For initial conditions close enough to the original centre the solution will experience some damping and, after a short interval of irregular oscillations, will become resonant (see Fig. 10).

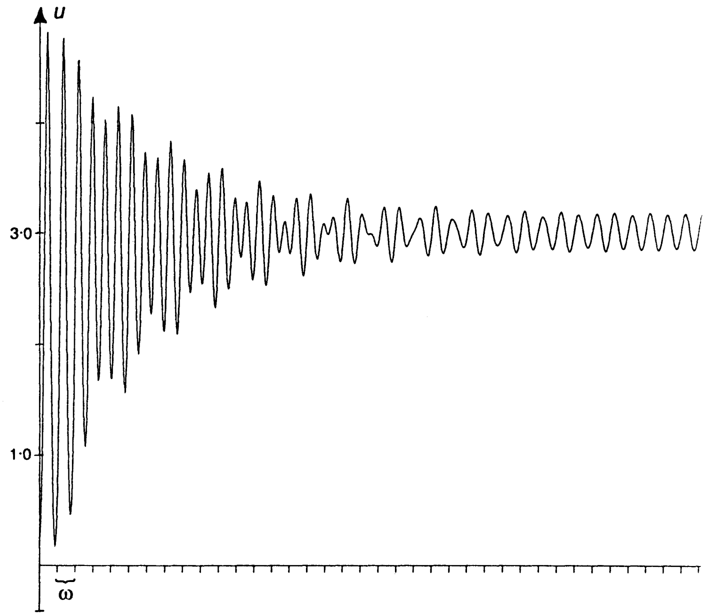

Fig. 10. Time series for the system (18).

5. Summary

The most relevant observation of this study is the fact that the Melnikov analysis on a degenerate three-dimensional system can be relegated to the set of reduced two-dimensional systems obtained by integration of the three-dimensional system and parametrised by the integration constant. As a result there is a set of homoclinic orbits embedded in the phase space of the three-dimensional system as depicted in Fig. 2*b*. This set corresponds to a set of soliton solutions which are more peaked (i.e. higher and narrower in wave form) for larger homoclinic orbits. The dissipative part of the perturbation applied modifies the solitons into shock waves which decay into damped oscillations, corresponding to the wave solutions for the KdV–Burgers equation; see Jeffrey and Kakutani (1972). The periodic part of the perturbation causes a sinusoidal wavetrain to interact with these modified solitons. It is important to note that for the Melnikov method to be applicable the phase velocity of this perturbing wave train must be equal to the velocity c in the travelling wave ansatz (see equation 8). This, however, does not mean that the velocity of the perturbing wave train is equal to the soliton or modified soliton phase velocity. In fact, as can be seen by the scale transformation shown by Jeffrey and

Kakutani (1972), the velocity of the travelling wave ansatz c and thereby the velocity of the perturbation has very little effect on the velocity of the original soliton. However, the effect of the perturbing wave train on the amplitude of the modified solitons depends on the ratio α/δ of perturbation amplitude α and dissipation coefficient δ for a given perturbation frequency ω. This effect is described by the relations (45), (46) and the accompanying bifurcation curves of Figs 3 and 4. The interpretation is that, when the ratio α/δ is less than the critical ratio α_c/δ_c, dissipation is the dominating effect causing temporary chaos, until the soliton is reduced to a periodic wave in resonance with the perturbing wave train, as can be seen in Fig. 10. The feature of temporary chaos occurs when the soliton undergoes a sequence of reversed saddle-node bifurcations (see equation 52) as it progresses to lower energy periodic waves, corresponding to closed periodic orbits in the phase portrait. At the critical ratio α_c/δ_c a bifurcation occurs and the soliton degenerates into unbounded oscillations. Above the critical ratio the behaviour is essentially the same except for a very short period of chaotic oscillations before the unbounded growth. Because transversal intersections of the invariant manifolds now occur, this chaotic behaviour can be explained by the Smale–Birkhoff homoclinic theorem.

Acknowledgments

It is the author's pleasure to thank Professor Delbourgo, who encouraged the project, for enlightening discussions. Useful suggestions for improvements from referee are also appreciated.

References

Birnir, B. (1988). *Physica* D **19**, 238.
Byrd, P. F., and Friedman, M. D. (1971). 'Handbook of Elliptic Integrals for Engineers and Scientists' (Springer: Berlin).
Gradshteyn, I. S., and Ryzhik, I. M. (1965). 'Table of Integrals, Series and Products' (Academic: New York).
Greenhill, A. G. (1892). 'The Applications of Elliptic Functions' (Macmillan: London).
Greenspan, B. D., and Holmes, P. (1983). *In* 'Nonlinear Dynamics and Turbulence' (Eds G. I. Barenblatt *et al.*), p. 173 (Pitman: London).
Guckenheimer, J., and Holmes, P. (1984). 'Nonlinear Oscillations, Dynamical Systems and Bifurcations of Vector Fields' (Springer: Berlin).
Holmes, P., and Marsden, J. E. (1981). *Arch. Rat. Mech. Anal.* **76**, 135.
Jeffrey, A., and Kakutani, T. (1972). *SIAM Rev.* **14**, 582.
Olver, P. (1986). 'Applications of Lie Groups to Differential Equations' (Springer: Berlin).
Shampine, L. F., Watts, H. A., and Davenport, S. M. (1976). *SIAM Rev.* **18**, 376.
Wiggins, S. (1988). 'Global Bifurcations and Chaos' (Springer: Berlin).

Appendix

To evaluate the bifurcation ratio R^m as given by (51) we first eliminate λ from (15) and the resonance condition (50) and obtain

$$[a(r_3-r_1)/(3b)]^{\frac{1}{2}} = \omega K(k)/\pi m; \qquad k^2 = (r_3-r_2)/r_3-r_1). \tag{A1}$$

This relation shows the dependence of the elliptic modulus k or the roots r_1, r_2, r_3 as given by (12) on the order of resonance m and the perturbation frequency ω. From (12) we can further derive by matching powers,

$$3/a = r_1 + r_2 + r_3, \quad -6k_1/a = r_1 r_2 + r_2 r_3 + r_3 r_1, \quad 6k_2/a = r_1 r_2 r_3 . \tag{A2}$$

The integration constant k_1 can be determined from (11) by substituting a given saddle position $(r_s, 0, 0)$ on the u axis:

$$k_1 = ar_s^2/2 - r_s . \tag{A3}$$

The integration constant k_2 varies within the set of periodic solutions (13) and therefore cannot be determined without knowing which solution becomes resonant for a given ω and m. The three determining equations for r_1, r_2, r_3 are therefore (A1) and the first two equations of (A2), which can be used to express two of the roots in terms of the third one and substitute them into (A1), which can now be solved numerically for k. This modulus so obtained can therefore be used to evaluate R^m via (51) assuming the given coefficients a, b, saddle position r_s, resonance order m and perturbation frequency ω.

Manuscript received 2 July, accepted 21 September 1990